# Exploring Sublimation as a Tool for Polymorphic Screening in Niflumic Acid-Caffeine Pharmaceutical Cocrystals

Francisco J. Acebedo-Martínez,\* Carolina Alarcón-Payer, Alicia Domínguez-Martín, Antonio Frontera, Rafel Prohens, Rafael Barbas, and Duane Choquesillo-Lazarte\*



Downloaded via UNIV DE GRANADA on October 24, 2025 at 10:38:14 (UTC). See https://pubs.acs.org/sharingguidelines for options on how to legitimately share published articles.

Cite This: https://doi.org/10.1021/acs.cgd.5c01007



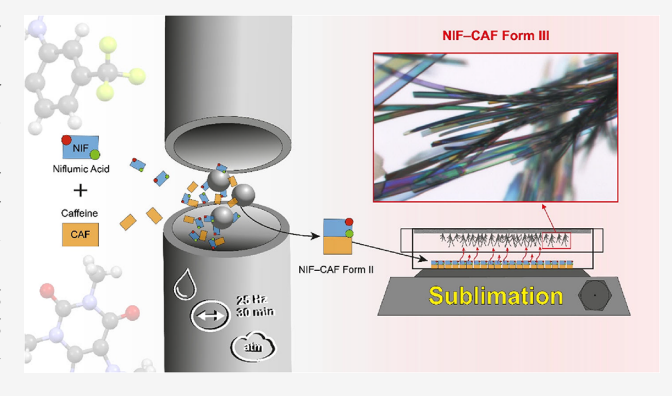
**ACCESS** I

Metrics & More

Article Recommendations

Supporting Information

ABSTRACT: Sublimation has emerged as a powerful tool for polymorphic screening in pharmaceutical multicomponent materials. In this work, a combined strategy involving mechanochemistry and sublimation enables the selective synthesis and isolation of a novel polymorph (Form III) of the niflumic acid-caffeine (NIF-CAF) cocrystal. Solid-state characterization and complementary theoretical studies revealed that Form III is morphotropically related to Form II, sharing a similar molecular conformation with the -COOH and -CF3 groups positioned on the same side of the NIF molecule. However, Form III exhibits a distinct packing arrangement, featuring embedded -CF3 groups and alternating molecular tapes stabilized by  $\pi - \pi$  and F...F interactions. Thermal analysis also indicates an enantiotropic relationship between Forms



II and III, with Form III becoming the more stable phase above the estimated transition temperature of ~102 °C, and showing a melting point of 156 °C. These findings demonstrate the relevance of sublimation in polymorphic screening and its potential to expand the solid-state landscape of multicomponent materials with enhanced control and reproducibility.

# 1. INTRODUCTION

Polymorphism plays a critical role in the pharmaceutical industry, as the bulk properties of active pharmaceutical ingredients (APIs) rely on the packing arrangements and the intermolecular interactions of their crystalline structure. 1,2 Moreover, polymorphism serves as a powerful strategy for modifying the properties of APIs without altering their chemical composition. However, it presents a significant challenge due to the complexity, diversity, and interconvertibility of polymorphic forms.<sup>3</sup> In fact, in 1965, McCrone affirmed that "... every compound has different polymorphic forms, and  $\cdots$  in general, the number of forms known for a given compound is proportional to the time and money spent in research on that compound".

In recent decades, pharmaceutical cocrystallization has emerged as a promising alternative to polymorphism for tailoring the physical and chemical properties of APIs by forming new multicomponent solid forms. 5-9 Initially, cocrystals were believed to offer a solution to the challenges of polymorphism, as interactions with a coformer could stabilize the API in a fixed crystalline structure, but this hypothesis was quickly discarded due to the increasing reports of polymorphic behavior even among cocrystals. 10-12

In our previous study, 13 we reported a polymorphic cocrystal of niflumic acid (NIF) and caffeine (CAF) (Figure 1) synthesized via mechanochemistry. We observed a clear

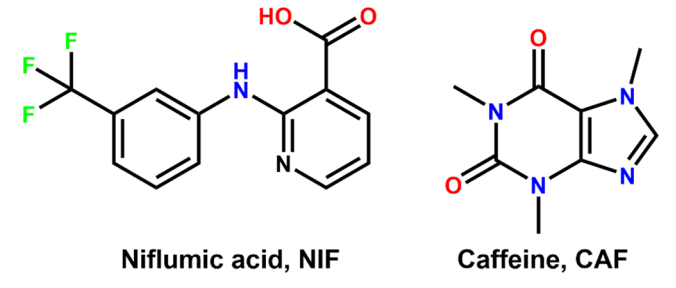


Figure 1. Molecular diagrams of niflumic acid (NIF) and caffeine (CAF).

temperature-dependent behavior in which NIF-CAF Form II converted into NIF-CAF Form I upon heating, which was followed by the sublimation of CAF, ascribed to the dissociation of Form I. These findings led us to investigate sublimation methodologies further to increase the polymorphic landscape of this system. Although sublimation is rarely used

Received: July 9, 2025 Revised: September 26, 2025 Accepted: October 1, 2025



for cocrystal synthesis, it is a solvent-free approach widely used for phase separation, controlling crystal morphology, and managing polymorphic transitions. 14–17

In this work, we aim to deepen our polymorphic understanding of the NIF-CAF system by exploring sublimation techniques. Specifically, our team combines Liquid-Assisted Grinding (LAG) with subsequent sublimation to isolate a novel polymorphic form of NIF-CAF with high purity. This approach will enable a detailed solid-state characterization and comparison with the previously reported cocrystals, with the broader goal of demonstrating the value of nontraditional crystallization methods in the discovery of novel pharmaceutical multicomponent materials.

## 2. EXPERIMENTAL SECTION

Niflumic acid (NIF), caffeine (CAF), and solvents were purchased directly from Sigma-Aldrich (purity >98%, Sigma-Aldrich, St. Louis, MO) and used as received.

**2.1. Synthesis of NIF-CAF Form III.** NIF-CAF III was obtained by sublimation of NIF-CAF II, prepared by LAG, following the already reported methodology. After confirming the purity of NIF-CAF II by Powder X-ray diffraction (PXRD), the initial microspacing in-air sublimation procedure search was carried out by placing 100 mg of the polymorphic cocrystal in a closed-glass Petri dish of 10 cm diameter and 0.5 cm in height. After heating the sample from the bottom of the plate at 135 °C for 3 h, suitable crystals for single-crystal X-ray diffraction (SCXRD) were isolated using a microtool and a microspatula, taking special attention not to take CAF crystals.

A second sublimation approach was performed under vacuum conditions in a 15 cm Schlenk tube. Again, 100 mg of NIF-CAF II was placed at the bottom of the tube with the help of a sonication bath. After 3 h of heating at 135 °C in an oil bath with a vacuum, suitable crystals were isolated and characterized by SCXRD.

**2.2. Characterization Techniques.** *2.2.1. X-ray Diffraction Analysis.* PXRD patterns were acquired with a Bruker D8 Advance Series II Vario diffractometer (Bruker-AXS, Karlsruhe, Germany) equipped with a Ge (111) primary monochromator and a LynxEye fast silicon strip detector. Generator operating conditions were 40 kV and 40 mA using Cu K $\alpha$  radiation. Measurements were performed in transmission geometry between Mylar foils with the beam focalized in the detector.

During SCXRD analysis, suitable crystals were prepared under inert conditions and immersed in perfluoropolyether as a protective oil for manipulation. Data collection was obtained at room temperature on a Bruker D8 Venture diffractometer (Bruker-AXS, Karlsruhe, Germany) using Cu K $\alpha$  radiation ( $\lambda$  = 1.54178 Å). The data were processed with the APEX4 suite.<sup>21</sup> The structure was solved with intrinsic phasing<sup>22</sup> and refined<sup>23</sup> with full-matrix least-squares on F<sup>2</sup> using Olex2 as a graphical interface.<sup>24</sup> The non-hydrogen atoms were refined anisotropically. Hydrogen atoms were located in difference Fourier maps and included as fixed contributions riding on attached atoms with isotropic thermal displacement parameters 1.2 or 1.5 times those of the respective atom. For the analysis and visualization of the structures, and also for graphic material preparation, Mercury software was used.<sup>25</sup> CIF file is deposited in the Cambridge Structural Database (CSD) under the CCDC number: 2451808. Copies of the data can be obtained free of charge at https://www.ccdc.cam.ac.uk/ structures/.

2.2.2. Theoretical Methods. The calculations of the noncovalent interactions were carried out using the Gaussian-16<sup>26</sup> and the PBE0-D3/def2-TZVP level of theory. <sup>27,28</sup> To evaluate the interactions in the solid state, crystallographic coordinates have been used. The interaction energies were computed by calculating the difference between the energies of isolated monomers and their assembly. The interaction energies were calculated with correction for the basis set superposition error (BSSE) by using the Boys–Bernardi counterpoise technique. <sup>29</sup> The Bader's "Atoms in molecules" theory (QTAIM)<sup>30</sup>

has been used to study the interactions discussed herein by means of the AIMall calculation package.  $^{31}$  The molecular electrostatic potential surfaces have been computed using the Gaussian-16 software.  $^{26}$ 

In order to assess the nature of interactions in terms of being attractive or repulsive and reveal them in real space, we have used the NCIPLOT index, which is a method for plotting noncovalent interaction regions, <sup>32</sup> based on the NCI (Noncovalent Interactions) visualization index derived from the electronic density. <sup>33</sup> The reduced density gradient (RDG), coming from the density and its first derivative, is plotted as a function of the density (mapped as isosurfaces) over the molecule of interest. The sign of the second Hessian eigenvalue times the electron density [i.e.,  $sign(\lambda_2)\rho$  in atomic units] enables the identification of attractive/stabilizing (bluegreen colored isosurfaces) or repulsive (yellow-red colored isosurfaces) interactions using two-dimensional (2D) Plots.

The interaction energy of each individual H-bond has been estimated using the potential energy density values at the bond CPs  $(V_r)$  and the equation proposed by Espinosa et al.  $(E = 0.5 \times V_r)$ . The lattice energy of the cocrystal was computed by creating a supercell composed of 32 molecules (16 of each coformer) by means of the Dmol3 program<sup>34</sup> as implemented in Materials Studio 2017.<sup>35</sup> For the calculation of the lattice energies, the isolated coformers in the gas phase were used. These calculations were performed using periodic boundary conditions, the PBE-D<sup>36</sup> functional, and the DNP basis set.<sup>34</sup> The numerical basis sets like DNP (double- $\zeta$  plus polarization) are more efficient than Gaussian basis sets and present negligible basis set superposition error.<sup>37</sup> The default DMol3 (implemented in Materials Studio 17.1.0.48) parameters were used for the calculations, which included a medium grid integration and a Self-Consistent Field (SCF) convergence of  $1 \times 10^{-5}$ . No vibrational analysis was performed. The raw energy values for all three polymorphs are listed in Table S1.

While the absolute values of the lattice energy estimations may carry some uncertainty due to the chosen combination of functional and basis set, the relative energies between the polymorphs are considered more reliable and can be confidently used for comparing their stabilities.

2.2.3. Thermal Analysis. Differential scanning calorimetry (DSC) analysis was carried out by using a Mettler-Toledo DSC-822e calorimeter. Experimental conditions: aluminum crucibles of 40  $\mu$ L volume, atmosphere of dry nitrogen with 50 mL/min flow rate, heating rates of 0.2, 1, and 10 °C/min. The calorimeter was calibrated with indium of 99.99% purity (mp 156.3 °C;  $\Delta H$  28.54 J/g).

Thermogravimetric analysis (TGA) was performed on a Mettler-Toledo TGA-851e thermobalance. Experimental conditions: alumina crucibles of 70  $\mu$ L volume, atmosphere of dry nitrogen with 50 mL/min flow rate, heating rates of 1 and 10 °C/min.

Hot-stage microscopy (HSM) was performed using a Nikon polarization microscope (Nikon Eclipse 50i) equipped with a Linkam LTS350 hot stage and a digital video recorder. Experimental conditions: atmosphere of dry nitrogen and heating rates of 1 and 10 °C/min.

2.2.4. Stability Studies. The stability of the polymorphs was evaluated and compared by slurry experiments in ACN, in which all of the polymorphic forms of this work are stable on their own. In these experiments, an excess of a mixture of NIF-CAF III and NIF-CAF I or II, in a ratio of 1:1, was placed in 1 mL of ACN for 24 h at room temperature, using sealed vials and magnetic agitation. The solids in the vials were collected, filtered, and dried at 35 °C for subsequent analysis by PXRD. The stability was also studied under accelerated aging conditions. For this purpose, 50 mg of solid was placed in a watch glass and stored at 40 °C and 75% RH (relative humidity) using a Memmert HPP110 climate chamber (Memmert, Schwabach, Germany). The stability of the sample was monitored by PXRD for 2 months.

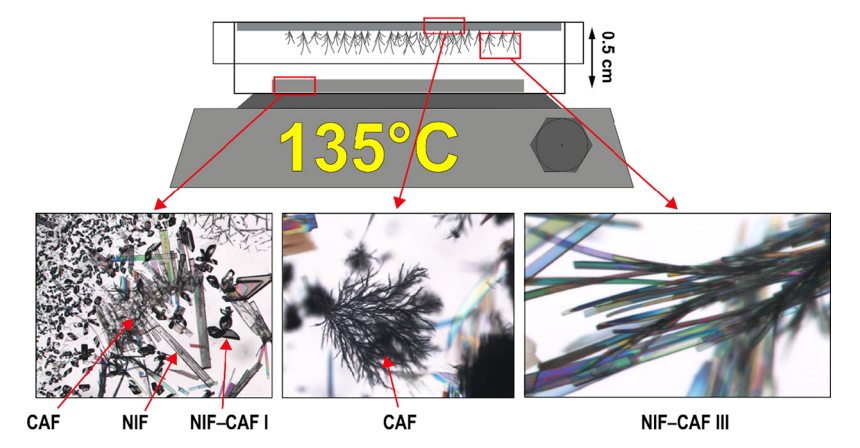


Figure 2. Schematic representation of NIF-CAF II sublimation procedure via microspacing in-air sublimation in a closed-glass Petri dish. Optical microscopy of NIF-CAF I, NIF, and CAF crystals at the bottom of the plate, and CAF and NIF-CAF III crystals at the top of the plate.

# 3. RESULTS AND DISCUSSION

**3.1. Synthesis of NIF–CAF Form III.** LAG strategies have shown remarkable potential for synthesizing multicomponent materials and screening their polymorphic forms. <sup>38–42</sup> Before this study, and to increase the polymorphic knowledge about the system **NIF–CAF**, a broad screening was performed by LAG, solution and crystallization techniques, but all resulted in the obtention of the already reported **Form I** and **Form II**. However, the observed thermal transitions of **Form II** into **Form I**, and the destabilization of the **NIF–CAF** system via CAF sublimation, denoted the impact of the temperature in this particular system, which led us to explore sublimation techniques for polymorphism screening.

Initially, the microspacing in-air sublimation approach was used in a closed Petri dish. This methodology has been reported for precise control over sublimation and deposition conditions, promoting the formation of high-quality single crystals with minimal material waste without the need for vacuum systems, inert gas environments, or sophisticated equipment, making it a practical and cost-effective approach for polymorph screening. <sup>20,18</sup>

Figure 2 illustrates the microspacing setup for the sublimation, in which NIF-CAF II was used as the starting material. After heating at 135 °C for 3 h, NIF-CAF I was found at the bottom of the plate, along with NIF crystals, indicating the complete transformation of Form II into Form I, and partial dissociation of Form I due to CAF sublimation, which confirmed the results obtained in our previous work.<sup>13</sup>

At the top of the Petri dish, we found CAF crystals along with long, thin crystals growing over them. SCXRD identified these as the new polymorph NIF-CAF Form III. The presence of NIF-CAF III, along with the absence of NIF crystals at the top of the dish, suggests that after the dissociation of Form I, the remaining NIF sublimed after CAF. The interaction of NIF vapor with a CAF-rich gas phase led to the cocrystallization of the novel NIF-CAF III. Interestingly, the crystals of this novel polymorph exhibited excellent flexibility, which is a characteristic typical of crystals obtained via microspacing in-air sublimation. <sup>19,43,44</sup> The PXRD patterns of all of the phases involved in the sublimation process are represented in Figure 3.

Similar experiments were performed by using Form I to evaluate the impact of the starting material. All trials resulted in the formation of NIF-CAF III over a layer of CAF. No significant influence of the starting material is observed from

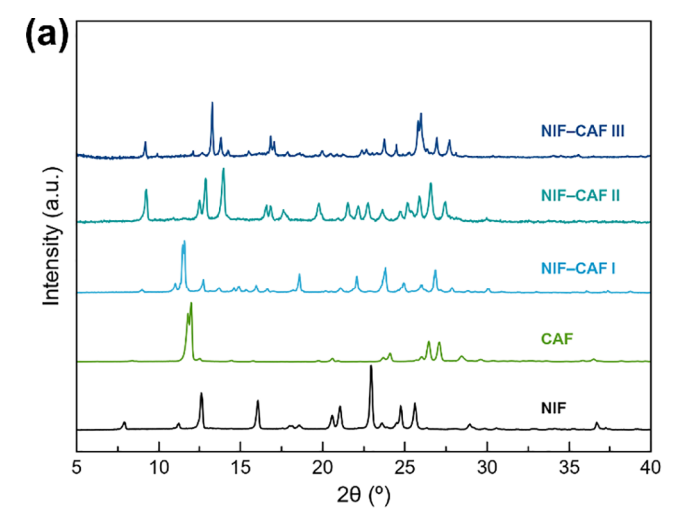


**Figure 3.** (a) PXRD patterns of the crystalline phases involved in the sublimation procedure.

these experiments, as Form II is transformed into Form I at 135 °C, followed by Form I's dissociation and CAF and NIF sublimation. Additionally, to determine whether NIF-CAF III could form directly from its components, we performed a cosublimation experiment using 141.11 mg of NIF and 97.10 mg of CAF in a 1:1 stoichiometric ratio. This approach also resulted in the formation of NIF-CAF III, but in significantly lower quantities than when starting with Forms I or II, and with a higher amount of CAF in the final bulk phase. This behavior is attributed to the ability of cocrystals to retard the sublimation of the pure components due to the stronger intermolecular interactions, increased lattice stability, and a stepwise release mechanism. 45-47 These features make cocrystals require more energy for sublimation, leading to a controlled and gradual release of CAF to the gas phase. In contrast, pure CAF sublimates rapidly due to its lower sublimation point, reducing the formation efficiency of NIF-CAF III. These findings suggest that NIF-CAF Form II, which is the direct product of LAG and can be obtained in higher quantities than Form I, is the most suitable starting material for synthesizing NIF-CAF III.

With a clear synthesis route established, the next step was to obtain a bulk phase for solid-state characterization. However, the initial polymorph screening indicated that NIF-CAF III is only accessible via gas-phase synthesis, and the microspacing

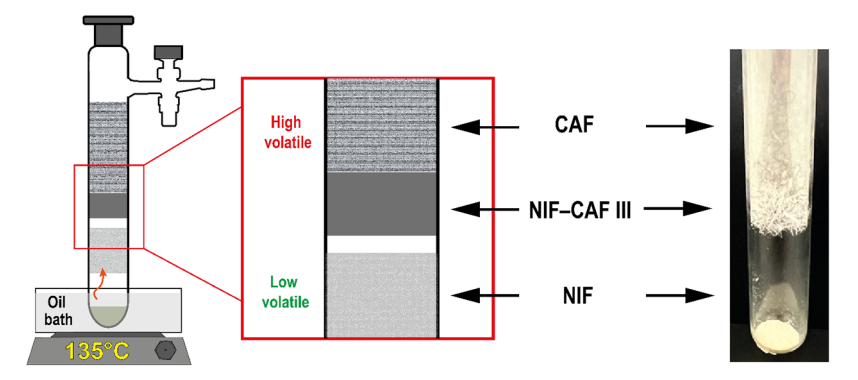


Figure 4. Schematic sublimation procedure in a Schlenk tube, for NIF-CAF III synthesis and separation.

in-air sublimation approach led to the formation of NIF-CAF III over a layer of CAF crystals, which makes the obtention of the novel polymorph in a pure state very complicated.

To solve these drawbacks, the sublimation process was refined to achieve an effective phase separation. We employed a sublimation setup using a Schlenk tube, a vacuum pump, and an oil bath to ensure uniform heating (Figures 4 and S1). Vacuum was applied to lower the NIF and CAF sublimation points, facilitating phase separation. One of the key advantages of this setup is the better spatial distribution of crystallized products along the inner walls, aiding in the collection of highpurity samples, and also vacuum-assisted sublimation accelerates sublimation rates, which may lead to uncontrolled crystal growth and limit reproducibility in large-scale synthesis.<sup>48</sup> In this approach, three distinct sublimation bands were observed along the walls of the Schlenk tube. These bands correspond to CAF, NIF-CAF III, and NIF, reflecting the differences in the volatility of the components, as shown in Figure 4. Interestingly, the morphology of the crystals was not altered, as long-thing-flexible crystals were obtained. This clear separation allowed the obtention of a pure phase suitable for further characterization. The purity of the phase was confirmed by comparing the PXRD of the sample obtained from sublimation with the simulated PXRD pattern obtained from the crystal structure (Figure S2).

**3.2. Crystal Structure Analysis.** The study via SCXRD of NIF-CAF Form III revealed certain common features with the previously reported Forms I and II, but also key distinctions. For a better comparison, Table 1 presents the main crystallographic features of the polymorphs in the NIF-CAF system, while Table S2 contains the complete crystallographic data for NIF-CAF Form III.

**Form III** crystallizes in the monoclinic system with the  $P2_1/$ n space group and a 1:1 stoichiometric ratio (Figure 5a) as its counterparts (Figure 6a,c). Additionally, Form III also follows the same arrangement of Form I and II, being characterized by a supramolecular heterosynthon formed between the carboxyl moiety of NIF and the imidazole ring of CAF (COO-H···N), replacing the typical carboxylic acid homosynthon of NIF, forming a dimer based on the  $R_2^2(7)$  graph set. <sup>49,50</sup> The dimers further assemble into molecular tapes, stabilized by a network of C-H···O and C-H···F interactions (Figure 5b), following a similar arrangement observed in Form II. Our previous studies have shown that the primary crystallographic difference between Form I and Form II arises from the rotation around the N10-C11 bond of the NIF molecule. Form I has its -CF<sub>3</sub> and -COOH on opposite sides ( $\tau = -173.51^{\circ}$ ), closely resembling the conformation of the original NIF, whereas in

Table 1. Crystallographic Data of the Polymorphic Cocrystals of System NIF-CAF

compound name	NIF-CAF I <sup>a</sup>	NIF-CAF II <sup>a</sup>	NIF-CAF III
CCDC number	2116472	2116473	2451808
Crystal system	monoclinic	monoclinic	monoclinic
space group	$P2_1/n$	$P2_1/n$	$P2_1/n$
a [Å]	8.618(3)	6.9667(4)	7.8915(3)
b [Å]	23.908(9)	8.1222(6)	7.0520(2)
c [Å]	10.872(4)	37.438(3)	38.3166(12)
$\alpha$ [ $^{\circ}$ ]	90	90	90
$\beta$ [ $^{\circ}$ ]	104.568(12)	94.400(4)	93.947(2)
γ [°]	90	90	90
volume [ų]	2168.1(14)	2112.2(2)	2127.29(12)

<sup>&</sup>lt;sup>a</sup>Crystallographic data are taken from Acebedo et al. <sup>13</sup>

**Form II** these substituents are on the same side ( $\tau = 8.26^{\circ}$ ), as also seen in **Form III**, indicating a conformational resemblance to **Form II** (RMSD = 0.3473, Figure S3).

Form I also presents a tape structure stabilized by  $C-H\cdots O$  and  $C-H\cdots F$  interactions, but the general arrangement differs from Form II and Form III, as shown in Figure 6b. Another key distinguishing feature of Form III is the spatial orientation of the  $-CF_3$  groups. Unlike in Form II, where these groups are prominently exposed at the periphery of the crystal lattice (Figure 6d), in Form III, they are embedded within the molecular framework, resulting in molecular tapes that are stacked and stabilized by multiple  $\pi\cdots\pi$  stacking and F···F interactions (Figure 5c).

The high volatility of CAF relative to NIF is a key feature of the sublimation process, leading to a CAF-rich gas phase that facilitates the formation of the NIF-CAF cocrystal upon desublimation. The columnar packing observed in NIF-CAF Form III, which is stabilized by  $\pi$ -stacking interactions between the alternating NIF and CAF molecules, can be rationalized by the nature of crystal growth from the gas phase. In this environment, directional interactions, such as hydrogen bonds and  $\pi$ -stacking, play a crucial role in directing the molecular assembly. The formation of one-dimensional (1D) columns, which is a common motif in crystals grown via sublimation, is often attributed to the energetic favorability of these strong, directional  $\pi - \pi$  interactions. The presence of these columnar structures in Form III suggests that the stacking interactions are kinetically favored during the rapid desublimation process, leading to the observed packing arrangement. This behavior is consistent with recent literature reports on the sublimation of other multicomponent systems,

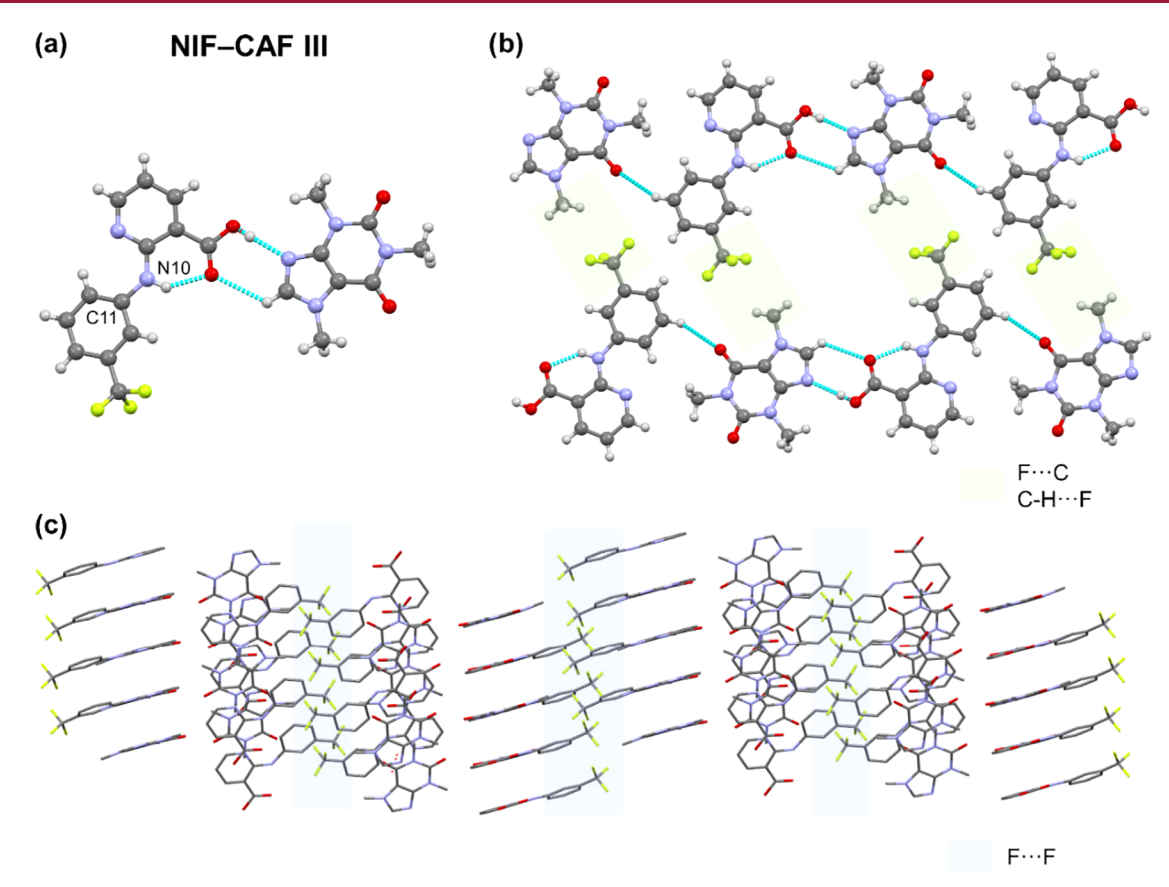


Figure 5. (a) Asymmetric unit of NIF-CAF III and (b) 2D tape structure of NIF-CAF III. Green boxes highlight the F···C and C-H···F interactions. (c) 3D crystal structure of NIF-CAF III. Blue boxes highlight the F···F interactions.

where the ability to form stable  $\pi$ -stacked columns is a critical factor in the formation of novel polymorphs.<sup>51</sup>

Additionally, Bravais-Friedel-Donnay-Harker (BFDH) morphology was calculated by using the BFDH method included in the latest release of the visualization software package Mercury<sup>52</sup> to compare with BFDH morphologies of the other two polymorphs previously reported (Figure 7). The calculated morphology is consistent with the experimentally observed crystal habits of both polymorphs: Form III grows as long, thin prismatic crystals, whereas Form II adopts a more voluminous prismatic shape. Furthermore, the analysis of noncovalent interactions supports that the maximal crystal growth is favored along the stacking direction, stabilized by  $\pi$ - $\pi$  interactions between alternating **NIF** and **CAF** molecules. This preferential growth axis rationalizes the columnar packing observed in Form III and explains its kinetic stabilization during the rapid desublimation process. Interestingly, although NIF-CAF III shows a very similar calculated morphology with respect to Form II with the same main faces: {002}, {00-2}, {101}, {-101}, {10-1}, and {-10-1} corresponding to 78 and 74% of the total surface, respectively, significant differences in the packing has been observed. In the case of Form II (Figure 7a), the predicted morphology shows that NIF and CAF molecules are disposed in well-defined channels (Figure 7b), but in Form III, both molecules are alternated and rotated almost 90° with respect to those of Form II (Figure 7d).

A detailed analysis of the packing revealed that both polymorphs can be considered morphotropes, since their packing motifs only differ by a noncrystallographic rotation of their common motifs.<sup>53</sup> Figure 8 shows layers formed by hydrogen-bonded caffeine/niflumic acid pairs in both Forms II and III. While in Form III, there is an alternate succession of layers related by inversion centers, in Form II, a noncrystallographic rotation of a layer with respect to Form III occurs, having only small intermolecular interaction consequences, keeping very similar cell parameters and predicted morphology.

On the other hand, Hirshfeld surfaces<sup>54</sup> and the associated fingerprint plot<sup>55,56</sup> were calculated from both **Forms II** and **III** to confirm the very similar pattern of intermolecular interactions and environment. As expected, no significant differences between the distribution of short contacts were observed (Figures 9, 10 and Table 2).

**3.3. DFT Study of Noncovalent Interactions.** A detailed analysis of the noncovalent interactions in NIF–CAF Form III was carried out to enable an accurate comparison with those of the other known polymorphs. To estimate the lattice energy of Form III, a supercell of 32 molecules (16 of each coformer) was used, along with periodic boundary conditions at the PBE–D/LNP level of theory. The resulting lattice energy is  $E_{\text{lattice}} = 69.8 \text{ kcal/mol}$ , which is comparable to those of the other two polymorphs previously reported by us, that are  $E_{\text{lattice}} = 70.5$  and 68.1 kcal/mol for Form I and II, respectively.

The most electron-rich and -poor parts of the reference APIs were previously investigated by computing their MEP surfaces. In addition, the MEP surface of the H-bonded heterodimer, a common synthon of all three forms, was used to investigate how the formation of the H-bond affects the  $\pi$ -stacking ability of the rings (Figure 11). In the heterodimer, upon formation of

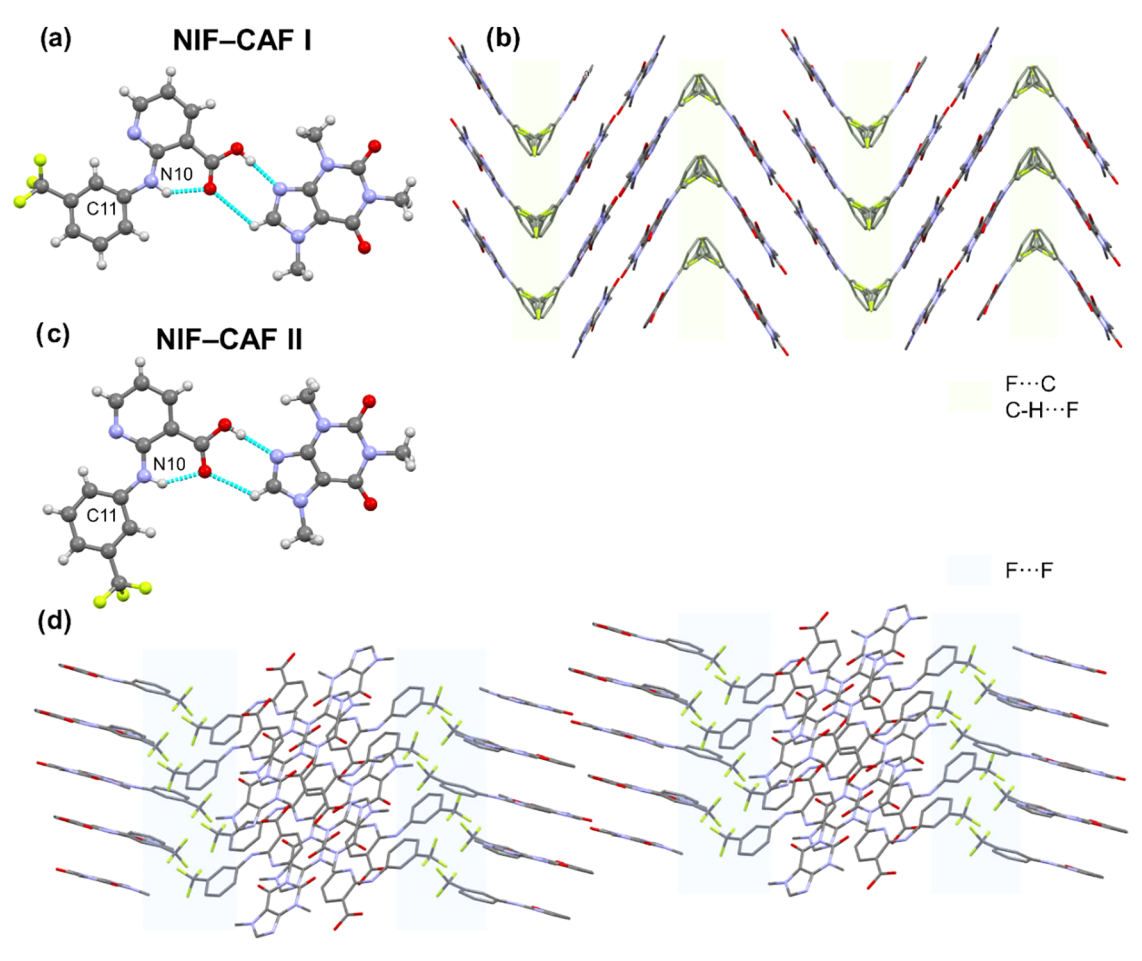


Figure 6. (a) Asymmetric unit of NIF-CAF I and (b) 2D tape structure of NIF-CAF I. Green boxes highlight the F···C and C-H···F interactions. (c) Asymmetric unit of NIF-CAF II and (d) 3D crystal structure of NIF-CAF II. Blue boxes highlight the F···F interactions.

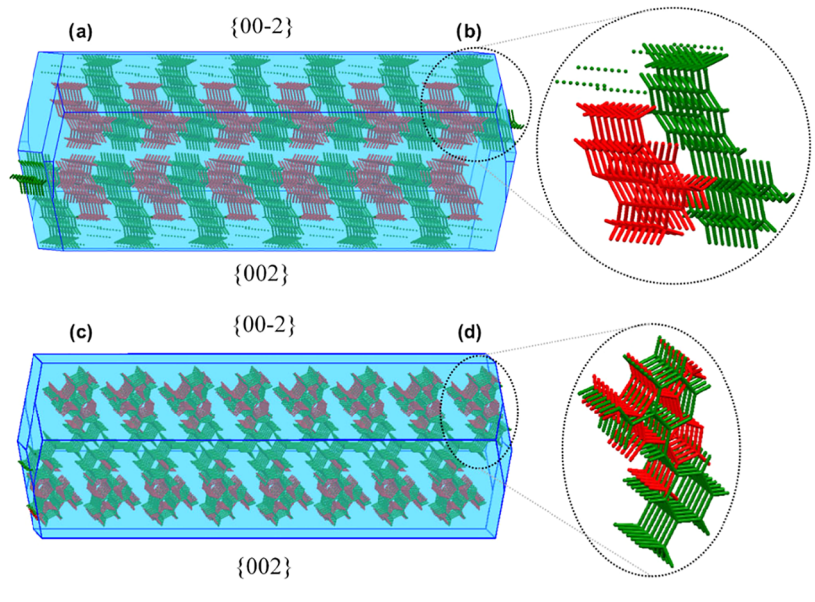


Figure 7. BFDH predicted morphology of (a) Form II and (c) III and (b, d) enlargement of NIF and CAF disposition, showing the largest faces. NIF molecules are represented in green and CAF molecules in red. {101}, {-101}, {10-1} and {-10-1} main faces are omitted for clarity.

the strong OH···N H-bond, the MEP values over the rings are significantly affected in the CAF coformer, increasing the  $\pi$ -acidity of both rings (11.9 and 12.6 kcal/mol, see Figure 11). In the NIF moiety, the MEP value over the carboxypyridine

ring is reduced to zero and remains unaltered in the phenyl ring. As detailed below, **Form III** establishes  $\pi$ -stacking assemblies where **CAF** and **NIF** interact via the pyrimidine and carboxypyridine rings, respectively. The fact that the MEP

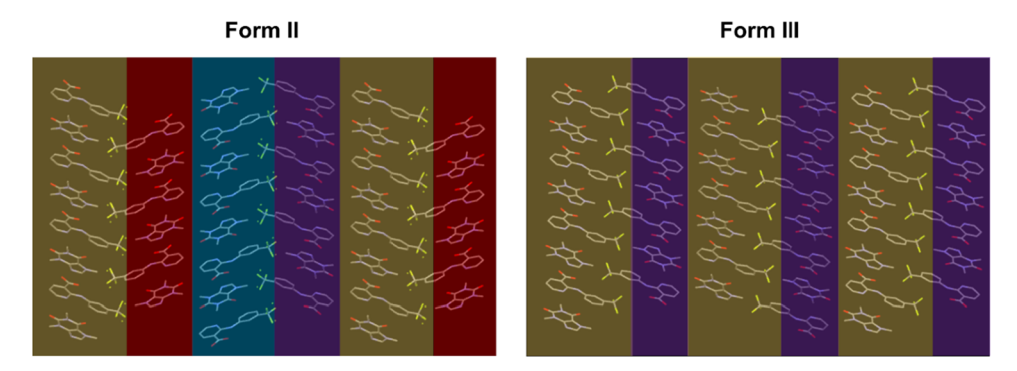


Figure 8. Alternate layers of hydrogen-bonded NIF/CAF pairs in Forms II and III. Layers with the same orientation in both forms are colored in yellow and purple, while those noncrystallographically rotated in Form II with respect to Form III are colored in red and blue.

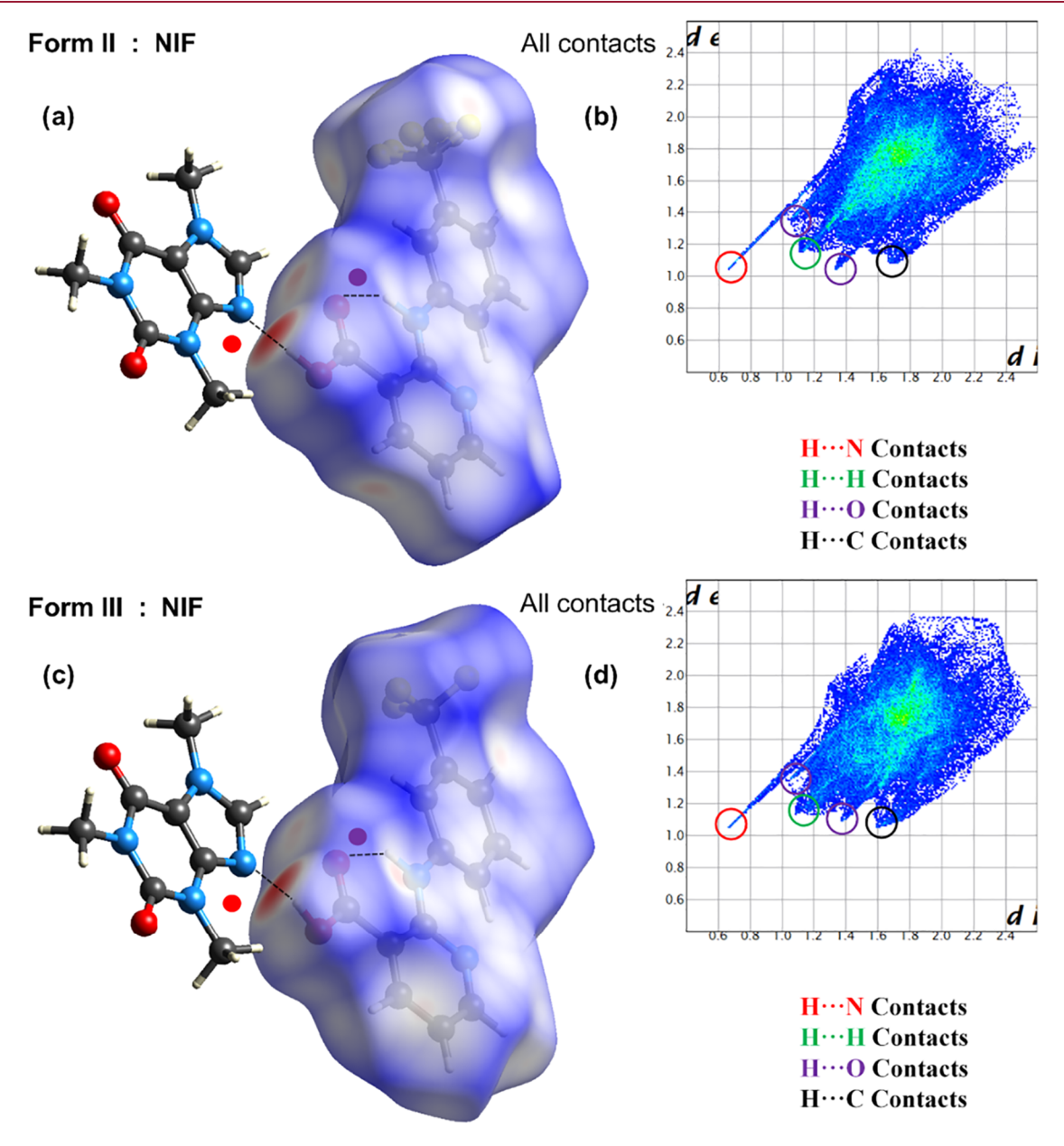


Figure 9. Representation of NIF···CAF interaction in Form II (up) and Form III (down), with (a, c) Hirshfeld surface mapped on NIF with  $d_{\text{norm}}$  and (b, d) fingerprint plots computed from Hirshfeld surfaces, strong H···N contacts are highlighted in red and H···O contacts in purple.

value at the carboxypyridine is reduced upon formation of the heterodimer facilitates the formation of this  $\pi$ -stacking by

eliminating the electrostatic repulsion and maximizing the attractive dispersion and polarization effects.

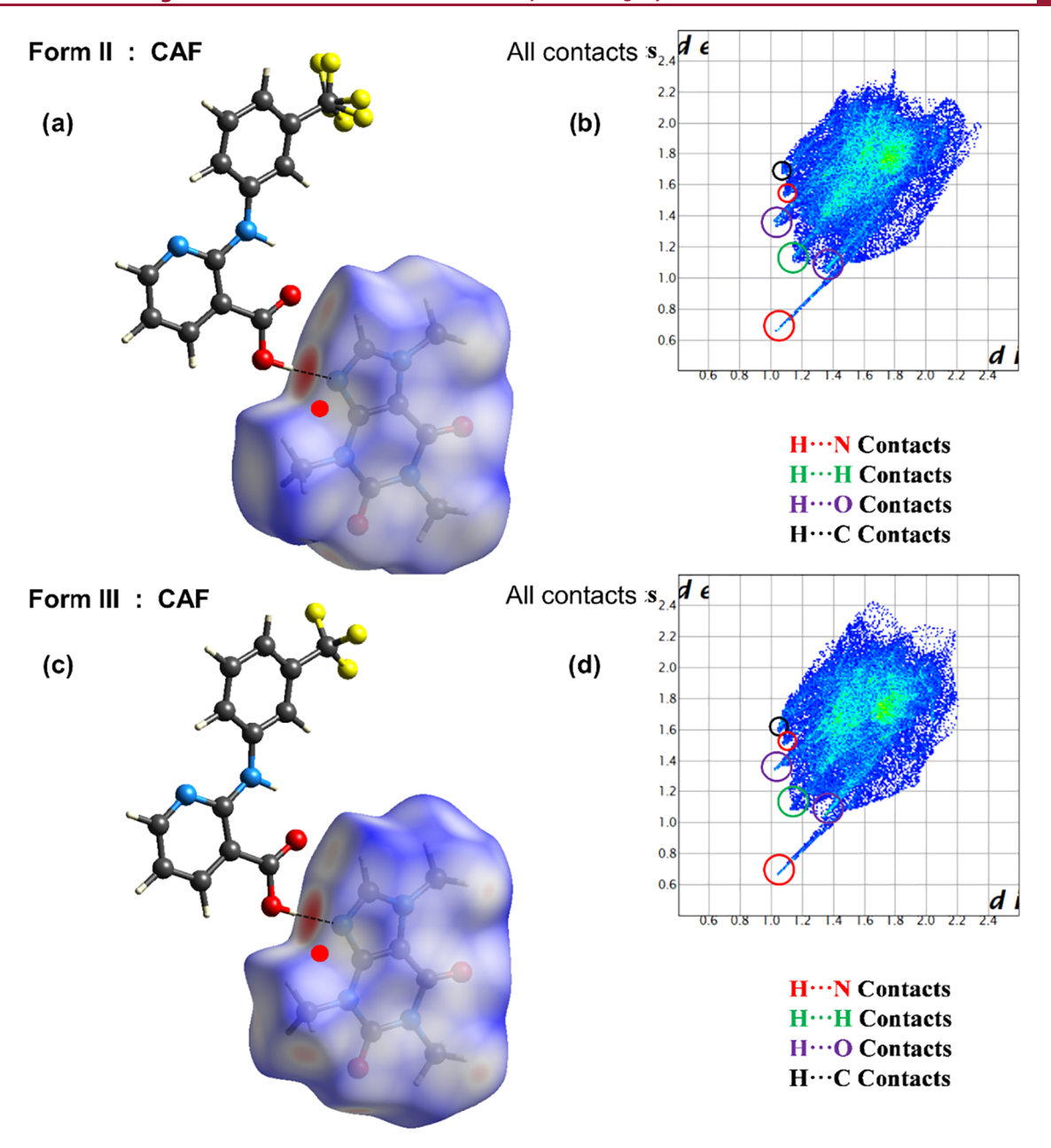


Figure 10. Representation of NIF···CAF interaction in the Form II (up) and Form III (down), with (a, c) Hirshfeld surface mapped on CAF with  $d_{\text{norm}}$  and (b, d) fingerprint plots computed from Hirshfeld surfaces, strong H···N contacts are highlighted in red and H···O contacts in purple.

Table 2. Surface Area Contribution (%) of the Main Intermolecular Contacts of NIF-CAF Form II and III

	niflumic acid molecules		caffeine molecules	
contacts	Form II	Form III	Form II	Form III
H⋯N	4.0	4.0	8.2	8.0
$H \cdot \cdot \cdot H$	29.3	29.9	35.9	34.6
H···O	13.4	13.7	18.0	18.8
H···C	11.7	11.1	10.1	12.6
$H \cdots F$	22.2	21.8	11.4	9.8

A recurrent  $R_2^2(7)$  H-bonded synthon is formed in all three **NIF-CAF** polymorphs. The distribution of bond and ring critical points (red and yellow spheres, respectively) and bond paths (represented as dashed bonds) of **NIF-CAF Form III** is shown in Figure 12, as well as superimposed NCIplot isosurfaces. The QTAIM analysis of the heterodimer

represented in Figure 12 resembles that of the previously reported NIF-CAF polymorphs, 13 showing two inter- and two intramolecular H-bonding interactions. The  $R_2^2(7)$  synthon is generated through the intermolecular contacts OH···N and CH···O, where the -COOH group of NIF interacts with the CAF coformer by using the N9 atom and the CH group of the imidazole moiety. Each H-bonding interaction is characterized by a bond CP and a bond path that connects the H atom to the N or O atom. They are also revealed by the RDG isosurfaces that are coincident with the location of the bond CPs. For the  $R_2^2(7)$  synthon, the RDG colors of the isosurfaces are dark blue and green for the OH···N and CH···O H-bonds, respectively, revealing strong and weak interaction, respectively. Coplanarity is induced in the aromatic moieties of NIF by intramolecular H-bonds. The individual hydrogen-bonding energies are indicated next to the bond CPs in Figure 12, where the strongest HB corresponds to the OH···N H-bond

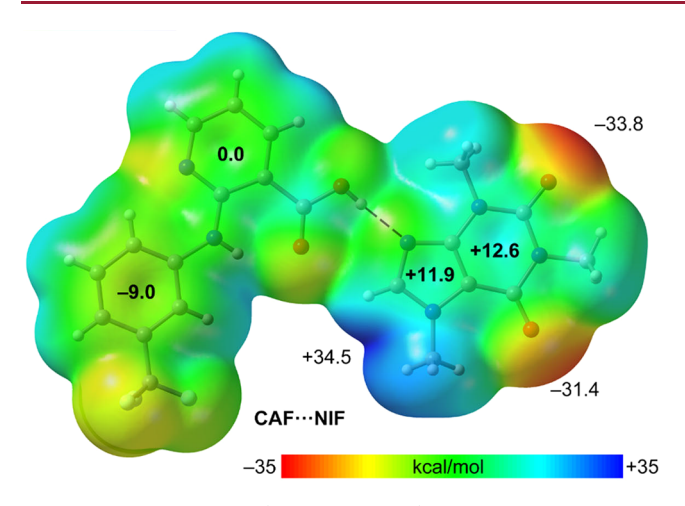


Figure 11. MEP surfaces (isovalue 0.01 au) of the heterodimer NIF-CAF at the PBE0-D3/def2-TZVP level of theory. The energies at selected points of the surfaces are given in kcal/mol.

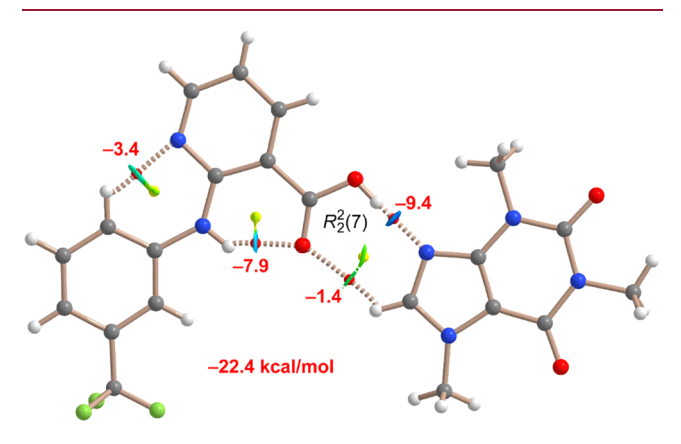


Figure 12. QTAIM distribution of bond and ring critical points (CPs, red and yellow spheres, respectively) corresponding to the H-bonds in NIF-CAF III. The strength of each individual H-bond is indicated next to the bond CPs. Superimposed NCIplot isosurfaces [s = 0.5, cutoff = 0.04 au, color scale -0.04 au (blue)  $\leq (\text{sign}\lambda_2)\rho \leq 0.04$  au(red)] are also indicated.

(-9.4 kcal/mol), as expected, followed by the intramolecular NH···O H-bond (-7.9 kcal/mol). The total energy due to the H-bonds is -22.4 kcal/mol (-11.3 kcal/mol corresponds to intramolecular H-bonds), which is similar to those reported for the previously reported polymorphs (-22.2 kcal/mol for Form I and -22.6 for Form II). The total interaction energy due to the  $R_2^2(7)$  synthon is very large (10.8 kcal/mol), thus confirming its relevance in the solid state of the novel polymorph and the formation of the heterodimer.

NIF-CAF III forms  $\pi$ -stacking assemblies in the solid state, as detailed in Figure 13, similar to those described for Form II. The RDG isosurfaces of the two tetrameric assemblies are shown in Figure 13. The presence of  $\pi$ -stacking interactions is evidenced by large green isosurfaces, in addition to the multitude of bond CPs and bond paths connecting the rings. The binding energy of the assemblies (considering the  $R_2^2(7)$  H-bonded dimer as a monomeric entity) is almost identical for both assemblies (-26.5 kcal/mol and -26.4 kcal/mol), which are slightly smaller (in absolute value) than those reported for Form I (-29.5 kcal/mol). In comparison to the H-bonding network depicted in Figure 12, the energies of the  $\pi$ -stacked assemblies are stronger, thus revealing the crucial role of  $\pi \cdots \pi$  interactions in the solid state of system NIF···CAF.

**3.4. Stability Studies.** *3.4.1. Thermal Stability.* DSC analysis has been used to study the relative thermal stability of Form III compared to previously reported Form I and II. <sup>13</sup> DSC of Form III shows a single endothermic phenomenon, which corresponds to the melting point, at 156 °C when heated at 10 °C/min (Figure 14).

The new polymorph has been found to be monotropically and enantiotropically related to Form I and Form II, respectively, based on the Burger and Ramberger's heat of fusion rule. Thus, Form III has a melting point very similar to Form I (156 °C) but a higher enthalpy of fusion (153.16 J/g for Form III against 145.70 J/g for Form I), and thus a monotropic relationship between both polymorphs can be assigned (DSC traces of Form I and Form II are presented in Figure S4). On the other hand, an enantiotropic relationship between Form II and Form III is observed based on the lower enthalpy of fusion of the higher melting point form, see Table 3. We have estimated the transition temperature between

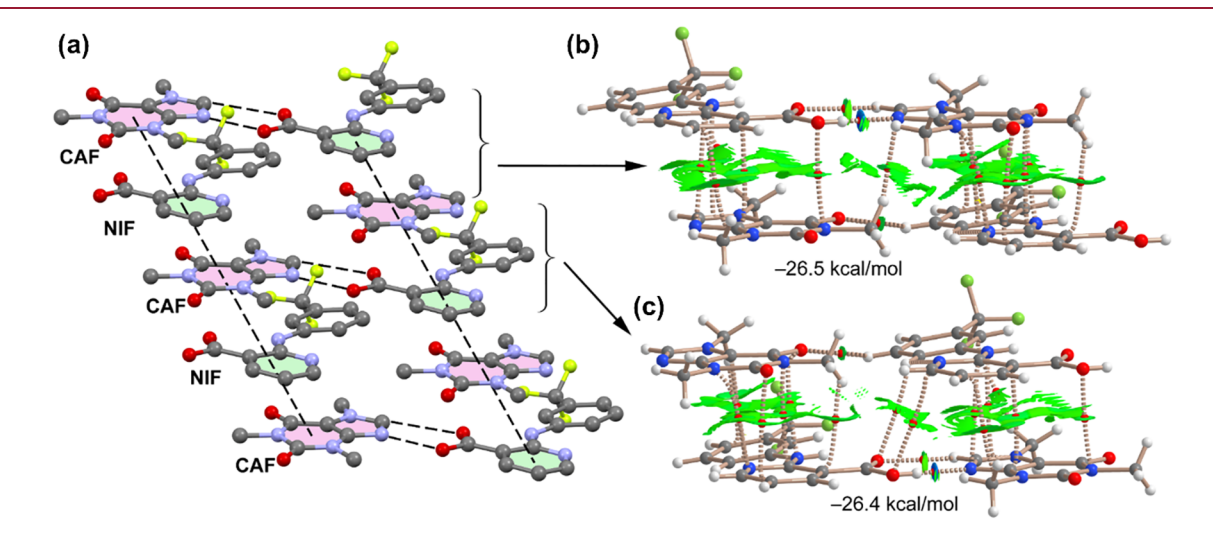


Figure 13. (a) Partial view of the X-ray packing of NIF-CAF III. (b, c) NCIplot isosurfaces [s = 0.5, cutoff = 0.04 au, color scale -0.04 au (blue)  $\leq (\text{sign}\lambda_2)\rho \leq 0.04$  au(red)] of the tetrameric assemblies extracted from the X-ray packing.

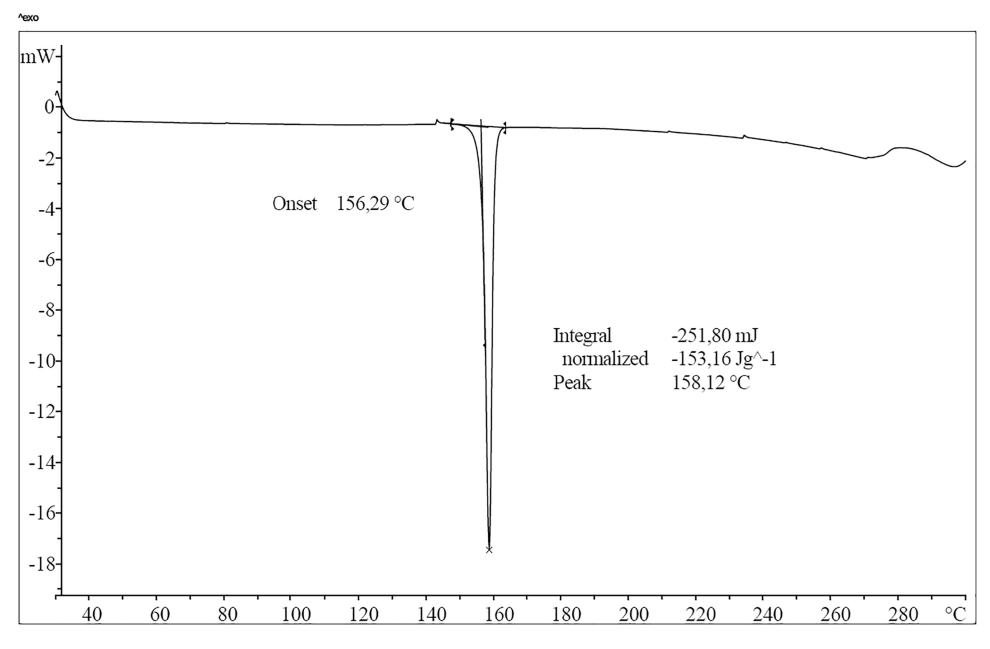


Figure 14. DSC thermogram of NIF-CAF Form III at a 10 °C/min heating rate.

Table 3. Parameters Used to Assess the Relative Stability of Polymorphs II and III

polymorph	melting point ( $^{\circ}$ C)	enthalpy of fusion $\left(J/g\right)$
I	157.68	145.70
II	152.17	161.84
III	156.14	153.16

polymorphs II and III from melting data<sup>58</sup> following the above-presented equation. The parameter k was fixed to 0.003,<sup>59</sup> and the theoretical value obtained by following this approach was 102 °C.

$$T_{\rm trs} = \frac{\Delta H_{\rm fus,2} - \Delta H_{\rm fus,1} + k \Delta H_{\rm fus,1} \left( T_{\rm fus,1} - T_{\rm fus,2} \right)}{\frac{\Delta H_{\rm fus,2}}{T_{\rm fus,2}} - \frac{\Delta H_{\rm fus,1}}{T_{\rm fus,1}} + k \Delta H_{\rm fus,1} \ln \left( \frac{T_{\rm fus,1}}{T_{\rm fus,2}} \right)}$$

Variable heating rate TGA analysis revealed from 30 to 165  $^{\circ}$ C a small loss of weight of 1.5%, similar to the other reported polymorphs, suggesting again sublimation of CAF in accordance with the same behavior observed in the other two polymorphs, Figure 15.

Variable hot-stage thermomicroscopy was carried out in order to further study its thermal behavior. When the new polymorph was subjected to the same first heating ramp as TGA analysis (10 °C/min until 140 °C), no changes were

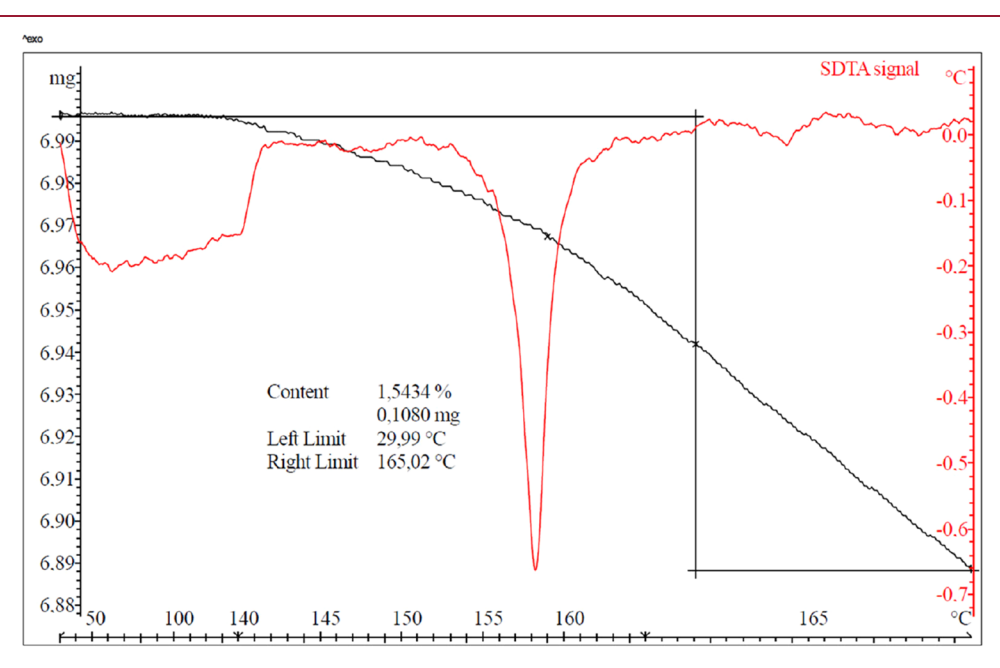


**Figure 15.** Variable heating rate TGA thermogram of **NIF–CAF Form III**. Method: first step from 30 to 140 °C at 10 °C/min heating rate, a second step from 140 to 165 °C at 1 °C/min heating rate, and finally a third isothermic step at 165 °C for 20 min. The SDTA signal is represented in red.

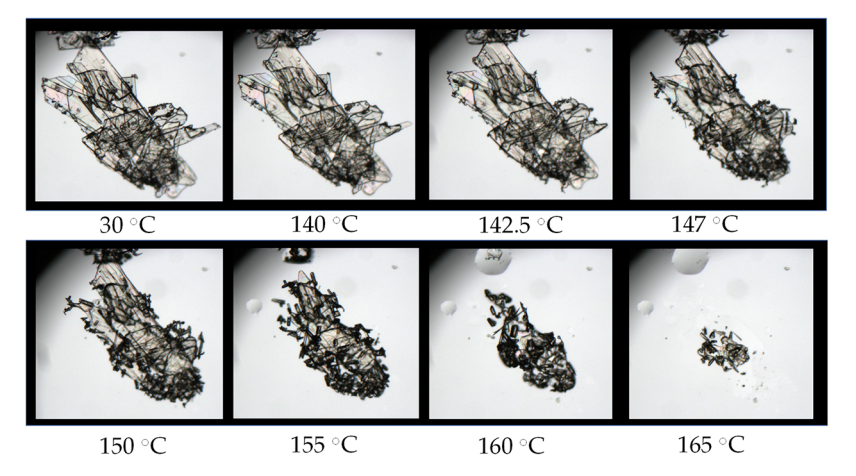


Figure 16. Microphotographs of the evolution of crystals of Form III when heated in a hot-stage.

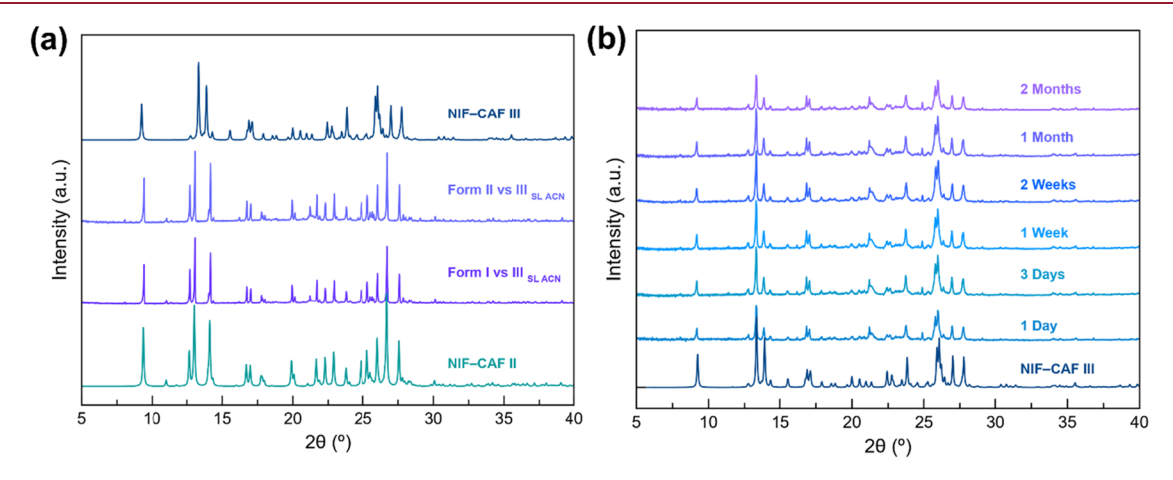


Figure 17. PXRD patterns of (a) the competence experiment in ACN and (b) NIF-CAF III accelerated aging conditions experiment for 2 months.

observed, but when it was subsequently heated at a heating ramp of 1 °C/min, the growth of new crystals from the surface of the existing ones was observed above 140 °C, followed by melting of the original crystals starting at 156 °C, the new ones remaining unchanged until 160 °C, when they started to melt (Figure 16). At this point, the sublimation of CAF is accompanied by the recrystallization of NIF, which was demonstrated by isolating and studying those crystals via SCXRD.

3.4.2. Thermodynamic Stability. To evaluate and compare the thermodynamic stability of the polymorphs, competence studies in 0.2 mL of ACN were performed by placing a stoichiometric mixture of Form III along with Forms I and II. After 24 h of agitation at room temperature, the powder was filtered, dried in air, and characterized by PXRD. Figure 17a represents the PXRD patterns obtained in these competence studies, which indicate that Form III converted into Form II, suggesting that Form II represents the thermodynamically most stable phase under these conditions. This transformation was consistent across all experiments, reinforcing the conclusion that Form II is the most stable polymorphic form at equilibrium in ACN.

Complementary stability studies under accelerated aging conditions were also performed at 40 °C and 75% RH over two months. The results shown in Figure 17b indicate that Form III remained unchanged, demonstrating stability under these conditions. This behavior was comparable to that of

Form I, which also maintained its integrity throughout the study. In contrast, our previous work demonstrated that Form II displayed excellent stability and also slightly better crystallinity retention, further supporting its role as the most stable phase.

The stability findings align well with the crystallographic characteristics of the polymorphs. The PXRD analysis and single-crystal data revealed that Form II has the most compact packing arrangement, contributing to its enhanced stability. The strong hydrogen-bonding network and well-ordered molecular stacking in Form II likely reduce the molecular mobility, making it less susceptible to transformations.

# 4. CONCLUSIONS

This study demonstrates the importance of sublimation for polymorph screening in multicomponent materials, allowing the obtaining of the novel NIF-CAF Form III. Moreover, a novel strategy that combines mechanochemistry, specifically LAG, and sublimation has been tested, providing significant advantages, including higher yield rates and improved purity. Among the different sublimation setups that have been evaluated, microspacing in-air sublimation provides the fastest and most cost-effective route, but it lacks purity control, whereas sublimation in a Schlenk tube under vacuum conditions allows better phase separation and the isolation of a pure bulk phase of NIF-CAF Form III. Additionally, the

crystal structure analysis reveals that **Form III** closely resembles **Form II**, while the density functional theory (DFT) calculations and the MEP analysis of the noncovalent interactions denote similarities with **Form I**, particularly in the  $\pi$ -stacking assemblies.

Finally, Form II was found to be the most thermodynamically stable, making it the most suitable candidate for pharmaceutical applications. Nonetheless, this study highlights the importance of exploring sublimation methods in the development of new pharmaceutical multicomponent materials, since techniques such as sublimation can lead to the discovery of alternative polymorphic forms, such as Form III, thereby expanding the polymorphic landscape of the system. These alternative forms may offer distinct advantages in terms of solubility, bioavailability, intellectual property, stability optimization, and the prevention of undesirable phase transitions—factors that are increasingly critical in the pharmaceutical industry.

## ASSOCIATED CONTENT

# **Supporting Information**

The Supporting Information is available free of charge at https://pubs.acs.org/doi/10.1021/acs.cgd.5c01007.

Comprehensive document: (1) Schlenk Tube sublimation set up for NIF-CAF Form III separation; (2) PXRD patterns of the product of the sublimation, compared with the pure components and the calculated powder pattern of the novel NIF-CAF Form III; (3) RMSD value of Niflumic acid in the polymorph II (blue) and polymorph III (red): 0.3473; (4) raw energies of polymorphs I-III computed using SP calculations of the X-ray coordinates (5) crystallographic data of NIF-CAF Form III (PDF)

# **Accession Codes**

Deposition Number 2451808 contains the supplementary crystallographic data for this paper. These data can be obtained free of charge via the joint Cambridge Crystallographic Data Center (CCDC) and Fachinformationszentrum Karlsruhe Access Structures service.

# AUTHOR INFORMATION

# **Corresponding Authors**

Francisco J. Acebedo-Martínez — Laboratorio de Estudios Cristalográficos, IACT-CSIC, 18100 Armilla, Spain; Email: j.acebedo@csic.es

Duane Choquesillo-Lazarte — Laboratorio de Estudios Cristalográficos, IACT-CSIC, 18100 Armilla, Spain; orcid.org/0000-0002-7077-8972; Email: duane.choquesillo@csic.es

#### **Authors**

Carolina Alarcón-Payer — Servicio de Farmacia, Hospital Universitario Virgen de las Nieves, 18014 Granada, Spain Alicia Domínguez-Martín — Department of Inorganic Chemistry, Faculty of Pharmacy, University of Granada, 18071 Granada, Spain; occid.org/0000-0001-8669-6712

Antonio Frontera — Departament de Química, Universitat de les Illes Balears, 07122 Palma, Spain; ◎ orcid.org/0000-0001-7840-2139

Rafel Prohens — Laboratory of Organic Chemistry, Faculty of Pharmacy and Food Sciences, University of Barcelona, 08028 Barcelona, Spain; orcid.org/0000-0003-0294-1720

Rafael Barbas — Unitat de Polimorfisme i Calorimetria, Centres Científics i Tecnològics, Universitat de Barcelona, 08028 Barcelona, Spain; orcid.org/0000-0002-1603-3689

Complete contact information is available at: https://pubs.acs.org/10.1021/acs.cgd.5c01007

#### **Author Contributions**

D.C.-L. designed the experiments. D.C.-L. and F.J.A.-M. supervised the project. C.A.-P., F.J.A.-M., A.D.-M., R.P, R.B., and A.F. conducted the experiments and analyzed the data. D.C.-L. and F.J.A.-M. prepared the manuscript. D.C.-L.: Funding acquisition. All authors revised the manuscript. All authors have read and agreed to the published version of the manuscript.

#### Notes

The authors declare no competing financial interest.

# ACKNOWLEDGMENTS

This research publication has been funded by the projects GBRMat PID2023-151538NB-I00, PID2023-146632OB-I00, and PID2023-148453NB-I00, supported by MCIU/AEI/ 10.13039/501100011033 and by "ERDF A way of making Europe".

## REFERENCES

- (1) Datta, S.; Grant, D. J. W. Crystal structures of drugs: advances in determination, prediction and engineering. *Nat. Rev. Drug Discovery* **2004**, *3*, 42–57.
- (2) Bernstein, J. Polymorphism in Molecular Crystals; Oxford University Press, 2007; Vol. 29.
- (3) Brittain, H. G. Polymorphism in Pharmaceutical Solids; CRC Press, 2018.
- (4) Fox, D.; Labes, M. M.; Weissberger, A.; Rice, S. A. Physics and Chemistry of the Organic Solid State, Volume 1. *Phys. Today* **1964**, 17, 76–78, DOI: 10.1063/1.3051554.
- (5) Babu, N. J.; Nangia, A. Solubility advantage of amorphous drugs and pharmaceutical cocrystals. *Cryst. Growth Des.* **2011**, *11*, 2662–2679.
- (6) Qiao, N.; Li, M.; Schlindwein, W.; et al. Pharmaceutical cocrystals: An overview. *Int. J. Pharm.* **2011**, 419, 1–11.
- (7) Aakeröy, C. B.; Forbes, S.; Desper, J. Using cocrystals to systematically modulate aqueous solubility and melting behavior of an anticancer drug. *J. Am. Chem. Soc.* **2009**, *131*, 17048–17049.
- (8) Schultheiss, N.; Newman, A. Pharmaceutical cocrystals and their physicochemical properties. *Cryst. Growth Des.* **2009**, *9*, 2950–2967.
- (9) Dai, X. L.; Chen, J. M.; Lu, T. B. Pharmaceutical cocrystallization: an effective approach to modulate the physicochemical properties of solid-state drugs. *CrystEngComm* **2018**, *20*, 5292–5316.
- (10) Aitipamula, S.; Chow, P. S.; Tan, R. B. H. Polymorphism in cocrystals: a review and assessment of its significance. *CrystEngComm* **2014**, *16*, 3451–3465.
- (11) Eddleston, M. D.; Sivachelvam, S.; Jones, W. Screening for polymorphs of cocrystals: a case study. *CrystEngComm* **2013**, *15*, 175–181.
- (12) Limwikrant, W.; Nagai, A.; Hagiwara, Y.; et al. Formation mechanism of a new carbamazepine/malonic acid cocrystal polymorph. *Int. J. Pharm.* **2012**, *431*, 237–240.
- (13) Acebedo-Martínez, F. J.; Alarcón-Payer, C.; Frontera, A.; et al. Novel polymorphic cocrystals of the non-steroidal anti-inflammatory drug niflumic acid: Expanding the pharmaceutical landscape.

Pharmaceutics **2021**, 13, No. 2140, DOI: 10.3390/pharmaceutics13122140.

- (14) McArdle, P.; Erxleben, A. Sublimation—a green route to new solid-state forms. *CrystEngComm* **2021**, 23, 5965–5975.
- (15) Lombard, J.; Smith, V. J.; Le Roex, T.; Haynes, D. A. Crystallisation of organic salts by sublimation: salt formation from the gas phase. *CrystEngComm* **2020**, *22*, 7826–7831.
- (16) Volkwyn, A. L.; Haynes, D. A. Crystallization of Organic Salts and Co-crystals by Sublimation: The Effect of Experimental Conditions. *Cryst. Growth Des.* **2023**, 23, 8212–8220.
- (17) Lombard, J.; Haynes, D. A.; Le Roex, T. Assessment of Cosublimation for the Formation of Multicomponent Crystals. *Cryst. Growth Des.* **2020**, *20*, 7840–7849.
- (18) Ye, X.; Liu, Y.; Han, Q.; et al. Microspacing In-Air Sublimation Growth of Organic Crystals. *Chem. Mater.* **2018**, *30*, 412–420.
- (19) Guo, Q.; Ye, X.; Lin, Q.; et al. Microspacing In-Air Sublimation Growth of Ultrathin Organic Single Crystals. *Chem. Mater.* **2020**, *32*, 7618–7629.
- (20) Li, H.; Wang, L.; Ye, X.; et al. Efficient Screening of Pharmaceutical Cocrystals by Microspacing In-Air Sublimation. *J. Am. Chem. Soc.* **2024**, *146*, 11592–11598.
- (21) APEX4 V202.1; Bruker-AXS: Madison, WI, USA, 2022.
- (22) Sheldrick, G. M. SHELXT—Integrated space-group and crystal-structure determination. *Acta Crystallogr., Sect. A: Found. Adv.* **2015**, 71, 3–8.
- (23) Sheldrick, G. M. Crystal structure refinement with SHELXL. Acta Crystallogr., C: Struct. Chem. 2015, 71, 3-8.
- (24) Dolomanov, O. V.; Bourhis, L. J.; Gildea, R. J.; Howard, J. A. K.; Puschmann, H. OLEX2: A complete structure solution, refinement and analysis program. *J. Appl. Crystallogr.* **2009**, *42*, 339–341.
- (25) Macrae, C. F.; Bruno, I. J.; Chisholm, J. A.; et al. *Mercury CSD* 2.0 new features for the visualization and investigation of crystal structures. *J. Appl. Crystallogr.* **2008**, *41*, 466–470.
- (26) Frisch, M. J.; Trucks, G. W.; Schlegel, H. B.et al. Gaussian 16, Revision C.01, Wallingford, CT, 2016.
- (27) Grimme, S.; Antony, J.; Ehrlich, S.; Krieg, H. A consistent and accurate ab initio parametrization of density functional dispersion correction (DFT-D) for the 94 elements H-Pu. *J. Chem. Phys.* **2010**, 132, No. 154104, DOI: 10.1063/1.3382344.
- (28) Weigend, F. Accurate Coulomb-fitting basis sets for H to Rn. *Phys. Chem. Phys.* **2006**, *8*, 1057–1065.
- (29) Boys, S. F.; Bernardi, F. The calculation of small molecular interactions by the differences of separate total energies. Some procedures with reduced errors. *Mol. Phys.* **1970**, *19*, 553–566.
- (30) Bader, R. F. W. A bond path: A universal indicator of bonded interactions. J. Phys. Chem. A 1998, 102, 7314-7323.
- (31) Keith, T. A. AIMAll TK Gristmill Software, Overland Park 2013.
- (32) Contreras-García, J.; Johnson, E. R.; Keinan, S.; et al. NCIPLOT: A program for plotting noncovalent interaction regions. *J. Chem. Theory Comput.* **2011**, *7*, 625–632.
- (33) Johnson, E. R.; Keinan, S.; Mori-Sánchez, P.; et al. Revealing noncovalent interactions. *J. Am. Chem. Soc.* **2010**, *132*, 6498–6506.
- (34) Delley, B. From molecules to solids with the DMol3 approach. *J. Chem. Phys.* **2000**, *113*, 7756–7764.
- (35) BIOVIA Materials Studio. https://www.3ds.com/.
- (36) Adamo, C.; Barone, V. Toward reliable density functional methods without adjustable parameters: The PBE0 model. *J. Chem. Phys.* **1999**, *110*, 6158–6170.
- (37) Inada, Y.; Orita, H. Efficiency of numerical basis sets for predicting the binding energies of hydrogen bonded complexes: Evidence of small basis set superposition error compared to Gaussian basis sets. *J. Comput. Chem.* **2008**, *29*, 225–232.
- (38) Fischer, F.; Scholz, G.; Benemann, S.; Rademann, K.; Emmerling, F. Evaluation of the formation pathways of cocrystal polymorphs in liquid-assisted syntheses. *CrystEngComm* **2014**, *16*, 8272–8278.
- (39) Fischer, F.; Heidrich, A.; Greiser, S.; et al. Polymorphism of Mechanochemically Synthesized Cocrystals: A Case Study. *Cryst. Growth Des.* **2016**, *16*, 1701–1707.

- (40) Hasa, D.; Jones, W. Screening for new pharmaceutical solid forms using mechanochemistry: A practical guide. *Adv. Drug Delivery Rev.* **2017**, *117*, 147–161.
- (41) Xiao, Y.; Wu, C.; Hu, X.; et al. Mechanochemical Synthesis of Cocrystal: From Mechanism to Application. *Cryst. Growth Des.* **2023**, 23, 4680–4700.
- (42) Trzeciak, K.; Dudek, M. K.; Potrzebowski, M. J. Mechanochemical Transformations of Pharmaceutical Cocrystals: Polymorphs and Coformer Exchange. *Chem. Eur. J.* **2024**, 30, No. e202402683.
- (43) Li, M.; Du, Q.; Zhang, Y.; et al. Flexible near-infrared polarized photodetector based on CuPc single crystal grown by microspacing in-air sublimation. *J. Mater. Chem. C* **2023**, *11*, 14456–14463.
- (44) Wang, Y.; Sun, L.; Wang, C.; et al. Organic crystalline materials in flexible electronics. *Chem. Soc. Rev.* **2019**, *48*, 1492–1530.
- (45) Li, X.; Liu, X.; Song, J.; et al. Drug-Drug Cocrystallization Simultaneously Improves Pharmaceutical Properties of Genistein and Ligustrazine. *Cryst. Growth Des.* **2021**, *21*, 3461–3468.
- (46) Zu, H.; Henry, R. F.; Zhang, G. G. Z.; MacGillivray, L. R. Inhibiting Sublimation of Thymol by Cocrystallization. *J. Pharm. Sci.* **2023**, *112*, 350–353.
- (47) Shi, J.; Zhang, Y.; An, Q.; Li, Y.; Liu, L. Improving the sublimation stability of ligustrazine with gallic acid by forming pharmaceutical cocrystal based on the Etter's rules. *J. Solid State Chem.* **2024**, 331, No. 124545.
- (48) Li, F.; Chen, S.; Hu, H.; et al. Crystallization Selectivity of Ribavirin Solution and Amorphous Phase. *Molecules* **2023**, 28, No. 6320.
- (49) Etter, M. C.; MacDonald, J. C.; Bernstein, J. Graph-set analysis of hydrogen-bond patterns in organic crystals. *Acta Crystallogr., Sect. B:Struct. Sci.* **1990**, *46*, 256–262.
- (50) Etter, M. C. Encoding and Decoding Hydrogen-Bond Patterns of Organic Compounds. Acc. Chem. Res. 1990, 23, 120–126.
- (51) Bryan, C. D.; Cordes, A. W.; Haddon, R. C.; et al. Molecular conductors from neutral-radical charge-transfer salts: preparation and characterization of an I doped hexagonal phase of 1,2,3,5-dithiadiazolyl ([HCN2S2].bul.). *J. Am. Chem. Soc.* 1994, 116, 1205–1210.
- (52) Docherty, R.; Clydesdale, G.; Roberts, K. J.; Bennema, P. Application of Bravais-Friedel-Donnay-Harker, attachment energy and Ising models to predicting and understanding the morphology of molecular crystals. *J. Phys. D: Appl. Phys.* 1991, 24, No. 89.
- (53) Kálmán, A. Morphotropism: link between the isostructurality, polymorphism and (stereo)isomerism of organic crystals. *Acta Crystallogr., Sect. B:Struct. Sci.* **2005**, *61*, 536–547.
- (54) Spackman, M. A.; Jayatilaka, D. Hirshfeld surface analysis. CrystEngComm 2009, 11, 19–32.
- (55) Spackman, M. A.; McKinnon, J. J. Fingerprinting intermolecular interactions in molecular crystals. *CrystEngComm* **2002**, *4*, 378–392.
- (56) McKinnon, J. J.; Jayatilaka, D.; Spackman, M. A. Towards quantitative analysis of intermolecular interactions with Hirshfeld surfaces. *Chem. Commun.* **2007**, 3814–3816.
- (57) Burger, A.; Ramberger, R. On the polymorphism of pharmaceuticals and other molecular crystals. I—Theory of thermodynamic rules. *Microchim. Acta* **1979**, *72*, 259–271.
- (58) Yu, L. Inferring thermodynamic stability relationship of polymorphs from melting data. *J. Pharm. Sci.* **1995**, 84, 966–974.
- (59) Lyon, R. E.; Walters, R. N.; Stoliarov, S. I. Thermal analysis of flammability. *J. Therm. Anal. Calorim.* **2007**, *89*, 441–448.